Global NEST Journal, Vol 24, No X, pp 1-10

Magnetic $CoFe_2O_4$@carbon yolk-shell nanoparticles as catalysts for the catalytic wet peroxide oxidation of paracetamol: kinetic insights

Guari N.M.C.[1,2], Silva A.S.[1], Diaz de Tuesta J.L.[1]*, Pottker W.E.[2], Cordeiro P.Y.[2] and Gomes H.T.[1]*

[1]Centro de Investigação de Montanha (CIMO), Instituto Politécnico de Bragança, Campus de Santa Apolónia, 5300-253 Bragança, Portugal

[2]Federal Technological University of Paraná (UTFPR), Avenida dos Pioneiros 3131, 86036-370, Londrina, PR, Brazil

Received: 20/03/2022, Accepted: 10/06/2022, Available online: 08/09/2022

*to whom all correspondence should be addressed: e-mail: htgomes@ipb.pt; jl.diazdetuest@ipb.pt

https://doi.org/10.30955/gnj.004309

Graphical abstract

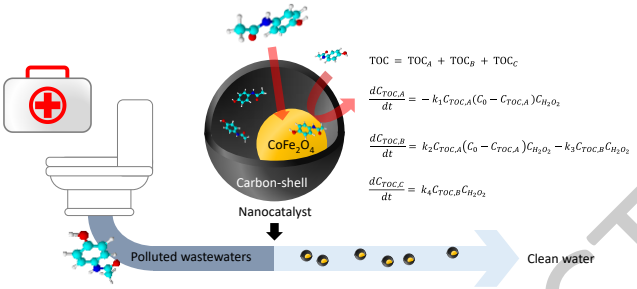

Abstract

This work focuses on the use of carbon-coated magnetic cobalt ferrite nanoparticles as catalysts for catalytic wet peroxide oxidation (CWPO) of the emerging concern pollutant paracetamol (PCM). The magnetic core of the catalyst is composed of $CoFe_2O_4$ developed by a sol-gel method. The core is subsequently coated with a formaldehyde-resorcinol resin and TEOS, further carbonized at 600°C, and etched with NaOH to create a yolk-shell structure denoted as $CoFe_2O_4$@void@C. X-ray diffraction (XRD), transmission electron microscopy (TEM), and Fourier transformed infra-red (FTIR) analysis revealed that the uncoated core is composed of a $CoFe_2O_4$ cubic spinel structure with a crystallite size of 53 nm calculated using the Williamson-Hall (W-H) method, matching very well the average size observed by TEM (53.51 $\pm$ 4.2 nm). Comparing the performances of $CoFe_2O_4$@void@C and the bare $CoFe_2O_4$ in the CWPO of paracetamol, total organic carbon (TOC) removals of 58% and 46% are obtained respectively after 24 h of reaction. An empirical kinetic model based on second-order and autocatalytic expressions was developed to suitably describe the decomposition of H_2O_2 and the removal of paracetamol using $CoFe_2O_4$@void@C as catalyst. The disappearance of TOC was well-described (r^2 = 0.98) by a lumped kinetic model as the sum of TOC_A, TOC_B and TOC_C, where TOCA is the TOC of the PCM, TOC_B refers the intermediate products and TOC_C is the TOC of the final products obtained during the CWPO of PCM.

Keywords: ferrite, nanostructure, nanocatalyst, advanced oxidation process, wastewater treatment, micropollutant, contaminant of emerging concern, acetaminophen, drug

1. Introduction

During the past decade, the European Union (EU) has been increasing efforts to monitor, control, and invest in research to find methods to eliminate pharmaceuticals of emerging concern in water matrices. The European Commission of 2015 established 10 pharmaceuticals to be monitored closely regarding their toxicity and possible threat in the aquatic environment, at the Union level (Decision/495/EC, 2015). Even though the amount of pharmaceuticals detected were in trace concentrations, they can cause a chain reaction of damage. This is because the pharmaceuticals have been found in water supplies to be affecting human life and also affecting the ecosystems, i.e., in the development of antibiotic-resistant microbes (Munoz *et al.*, 2017; Gadipelly *et al.*, 2014). Among contaminants of emerging concern across the EU, paracetamol (acetaminophen or 4-acetylaminophene-nol) is extensively used as a pain reliever and reducing fever (Van *et al.*, 2020). It deserves special attention regarding its effects of toxicity on humans and the environment because, as other pharmaceuticals, paracetamol can not be retained in conventional wastewater treatment plants (WWTP) (Silva *et al.*, 2019; Huaccallo-Aguilar *et al.*, 2021). Furthermore Zhang *et al.*, 2019, demonstrated the extensive impact of paracetamol in the endocrine interference to the body, as well as its nefarious effects to the environment. Therefore, this work seeks to transform paracetamol into more bio-degradable forms such as CO_2 and H_2O from the CWPO reactions.

The development of new efficient and economically viable technologies for the treatment of water containing pharmaceuticals has been widely investigated. Advanced

oxidation processes (AOPs) appear as an answer with low cost and relative ease of reproduction. Among AOPs, catalytic wet peroxide oxidation (CWPO) is a technique that can be characterized by the employment of hydrogen peroxide (H_2O_2) as an oxidation source, with a suitable catalyst to promote its partial decomposition into hydroxyl radicals ($HO^{\bullet}$). Magnetic materials can be applied directly as catalysts or included in different support/hybrid materials in CWPO (Diaz de Tuesta *et al.*, 2021; Diaz de Tuesta *et al.*, 2020; Huaccallo-Aguilar *et al.*, 2021, Duan *et al.*, 2017; Munoz *et al.*, 2020).

In this study, the hybrid carbon material can promote the decomposition of hydrogen peroxide into hydroxyl radicals, which are responsible for oxidizing the pollutants. In this case, the catalyst can be recovered at the end with the application of a magnetic field. Also, if the catalyst is stable enough, it won't generate dangerous levels of iron leaching and will lead to a shorter time of catalytic reaction (Huaccallo-Aguilar *et al.*, 2021;. Huaccallo-Aguilar *et al.*, 2021).

Due to their importance in catalysis, previous studies on ferrites nanoparticles (NPs), such as cobalt ferrites $CoFe_2O_4$, have been intensively investigated especially in terms of structural and morphological properties, as well as the synthesis procedures. $CoFe_2O_4$, when used as a heterogeneous catalyst for water treatment (Ribeiro *et al.*, 2018; Ribeiro *et al.*, 2017, Cai *et al.*, 2020), has shown remarkable chemical stability, large magnetic anisotropy, moderate saturation magnetization, and predominantly ferromagnetic behavior (Giannakopoulou *et al.*, 2002; Pullar, 2012; Ribeiro *et al.*, 2018; Ribeiro *et al.*, 2017). These characteristics contribute to easy separation of the catalyst from the water matrices at the end of treatment, upon the application of a magnetic field through the system (Heidari *et al.*, 2019; Kim *et al.*, 2016; Senapati *et al.*, 2012).

There are several methods to produce ferrites. The sol-gel method is a technique with high reproducibility, the control of the structural and morphological properties, and the certainty of obtaining a magnetic nanomaterial (Kiani *et al.*, 2021; Dippong *et al.*, 2021; Giannakopoulou *et al.*, 2002). After the sol-gel synthesis, heat treatment is necessary to ensure the nanomaterial thermo-stability.

The scientific community has been investigating the effects of using carbon to coat the catalysts used in industrial water treatment. This interest is due to the specific properties of carbon as a stabilizer agent in basic and acidic media, its high surface area, which allows high dispersion and stability for supported metals, as well as the possibility to control the morphological properties of the final composite (Oliveira *et al.*, 2018; Ribeiro *et al.*, 2016; Rodrigues *et al.*, 2018, Masudi *et al.*, 2020). However, the most important properties in this study are the increase of the catalyst recovery rate and the elimination/reduction of metal leaching from the catalyst to the treated waters.

The present work aims to develop carbon-coated catalyst composites constituted of yolk-shell cobalt ferrite NPs $CoFe_2O_4$@void@C for application in CWPO of water streams containing the model pollutant paracetamol. Also, an empirical kinetic model was developed to study the decomposition of H_2O_2, the removal of paracetamol, and the Total Organic Carbon (TOC) rate.

2. Materials and methods

2.1. Reagents

For the synthesis of the magnetic core, iron (III) chloride hexahydrate (99%, Merck), cobalt (II) chloride hexahydrate (99%, Fisher Chemical), ethylene glycol (99.5%, Fluka Analytical) and ethanol absolute (99.8%, Fisher Scientific) were used. Tetraethyl orthosilicate (TEOS, 98%, Fluka), resorcinol (99%, Fisher Scientific) and formaldehyde (37-38% wt., Panreac) were used for the coating of the NPs. To remove the silica, sodium hydroxide (99.1%, Fisher Scientific) was used.

The CWPO runs were performed using paracetamol (98%, Alfa Aesar), hydrogen peroxide (30% w/v, Fisher Chemical), and sulfuric acid (98%, Panreac). For analytical techniques, ortho-phosphoric acid (85%, Riedel-de Haen), and titanium (IV) oxysulfate (15 wt% in dilute sulfuric acid 99.99%).

All reagents were used without further purification and, ultrapure water and ethanol absolute (99.8%, Fisher Scientific) were used as solvents throughout this work.

2.2. Synthesis of $CoFe_2O_4$ yolk-shell NPs

The magnetic core ($CoFe_2O_4$) was synthesized according to the Sol-gel methodology described by Giannakopoulou *et al.*, 2002. In this methodology, the metal precursor undergoes rapid hydrolysis to produce a metal hydroxide solution, with a consecutive condensation leading to formation of a three-dimensional gel structure. The gel is dried and the resultant solid is calcined to remove organic impurities. The carbon-based yolk shell architecture was achieved by a sequential procedure summarized in coating, annealing, and etching. The coating consisted in a one-pot strategy for the synthesis of YS nanoparticles by hydrolysis of TEOS and polymerization of the precursors 1,3-benzenediol (resorcinol) and methanal (formaldehyde). Annealing was performed in inert (N_2) atmosphere at 120 and 400 °C for 1 h at each temperature, and 600 °C for 4 h. At last, silica was removed to achieve YS architecture upon etching with NaOH 10 M solution during 16 h. Coating conditions were the same as used in previous works, and described in more detail by Rodrigues *et al.*, 2018.

2.3. Characterization techniques

Structural characterization and average crystallite size were measured by X-ray Diffraction (XRD) using Cu-K_α radiation (λ = 0.15nm) in a Bruker D8 Discover diffractometer. *Transmission* Electron Microscopy (*TEM) was performed in an H-9000 instrument operating at 300 kV. ImageJ software (*NIH, Bethesda, MD, USA*) was used to estimate the size of the magnetic NPs.* Fourier Transform Infrared Spectroscopy (FTIR) spectra of the $CoFe_2O_4$@void@C sample were recorded on a Perkin Elmer FT-IR spectrophotometer UATR two infrared spectrophotometer, with a resolution of 4 cm^{-1}.

2.4. CWPO experiments

Batch CWPO runs of PCM were performed in a stirred glass reactor. The reactor was loaded with 100 mL of PCM solution ($C_{PCM,0}$ = 0.6615 mmol·L^{-1}) acidified until pH 3.5 employing H_2SO_4, and 0.25 g of catalyst. 158 µL of a 30%w/v peroxide solution was then added to obtain the concentration of H_2O_2 required for complete mineralization of PCM ($C_{H_2O_2,0}$ = 13.8881 mmol·L^{-1}). The controller maintained the temperature at 80 °C. In this study, pH and temperature were the same for all experiments, and were chosen based on previous observations to maximize H_2O_2 conversion into hydroxyl radicals (Diaz de Tuesta, Quintanilla, Casas, *et al.*, 2020). The samples were periodically withdrawn at selected times from 5 to 1440 min to analyze PCM degradation, H_2O_2 consumption, TOC abatement and iron leached from catalysts, following the methodology described in previous works (Silva *et al.*, 2019; Diaz de Tuesta *et al.*, 2021). Percentage of iron leached was calculated considering the mass of reagents used to synthesize the magnetic nanoparticle and the mass of iron leached at the end of experiments.

The kinetic study of the oxidation was carried out as detailed in previous works (Diaz de Tuesta *et al.*, 2021; Diaz de Tuesta *et al.*, 2019; Quintanilla *et al.*, 2019).

3. Results and discussion

3.1. Characterization of ferrite nanocatalyst

Figure 1 shows the XRD patterns of the core $CoFe_2O_4$ and $CoFe_2O_4$@void@C powders samples, prepared by sol-gel method. The position and relative intensities of the peaks correspond well to the standard XRD pattern of $CoFe_2O_4$ indicating retention of the crystalline cubic spinel structure during funcionalization with carbon-coated.

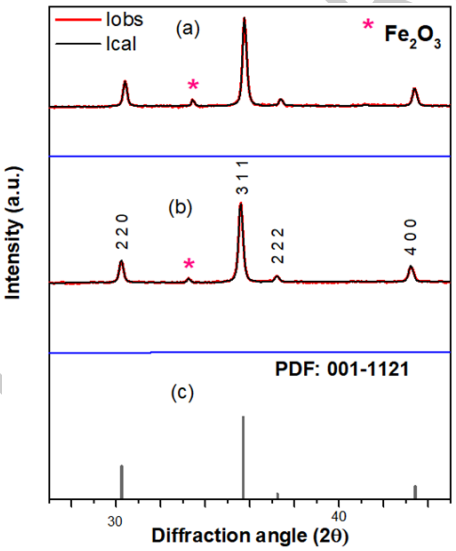

Figure 1. XRD diffractograms of the (a) core $CoFe_2O_4$, (b) $CoFe_2O_4$@void@C and, (c) reference cards.

As it can be observed, the diffraction peaks of the XRD pattern can be indexed to $CoFe_2O_4$ cubic spinel structures with space group Fd-3m (JCPDS Card No 001-1121). After coating, the catalyst structure remained the same, as shown by the characteristic peaks.

An analysis with the Rietveld method (Rietveld, 1969) confirmed that the face-centered cubic spinel structure of synthesized cobalt ferrite is present in the nanoparticles, coexisting with a secondary phase corresponding to 4.7 % of Fe_2O_3 (JCPDS Card No 024-0072).

The results of the Rietveld refinement for all samples are summarized in Table 1.

Table 1: The values of the refined lattice parameters, unit cell volume, crystalline size, average grain size of the samples as-prepared.

Samples	Lattice constant a (Å)	Volume (Å3)
$CoFe_2O_4$	8.393	591.223
$CoFe2O_4$@void@C	8.393	591.223

In particular, the crystallite size of the prepared $CoFe_2O_4$ powders is 53.3 ± 0.6 nm, as calculated by the Williamson-Hall method (W-H) (Hall, 1949; Nath *et al.*, 2020). The TEM image presented in Figure 2a shows the bare cobalt ferrite core synthesized through the sol-gel method with an average size of 53.5 ± 4.2 nm, in agreement with the value obtained by the W-H method from the XRD spectrum. The observed agglomeration is related to the ferromagnetic characteristics of the sample. By the shape and morphologies of $CoFe_2O_4$@void@C observed in Figure 2b, the lighted shadowy border evidences the coating of the magnetic NPs and the cobalt ferrite core shelled by a carbon-based layer, as observed elsewhere (Ribeiro *et al.*, 2017; Rodrigues *et al.*, 2018; Zhang *et al.*, 2010). The nanoparticle's size increased to 58.7 ± 8.1 nm according to TEM results, as expected due to carbon coating and void.

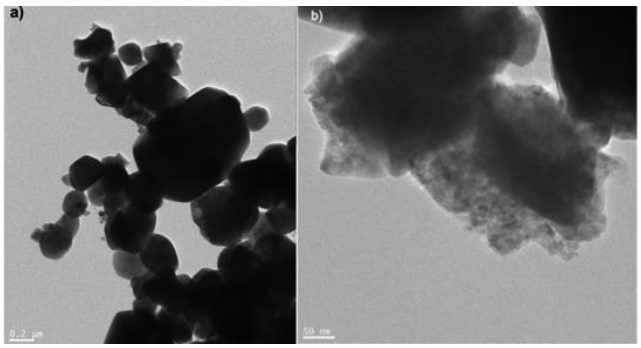

Figure 2. TEM image of the: a) magnetic core ($CoFe_2O_4$); b) $CoFe_2O_4$@void@C.

The morphological properties found in this work agree so far with other studies of synthesis of NPs. The work reported by Ribeiro *et al.*, 2017 about the preparation of magnetite, nickel, and cobalt ferrites encapsulated within graphitic shells shows similar results. The core-shell structures of $NiFe_2O_4$/MGNC and $CoFe_2O_4$/MGNC had a crystallite size of 33 ± 5 and 33 ± 2 nm, respectively. The average size of the nickel and cobalt ferrites is 36 ± 15 and 56 ± 18 nm, respectively determined from TEM measurements. Desai *et al.*, 2020 reported a study regarding the Zn-Zr co-substitutes cobalt ferrite nanoparticles ($CoZn_xZr_xFe_{2-2x}O_4$, x = 0 – 0.4) synthesized by sol-gel auto-combustion route. The formation of the cubic phase of $CoFe_2O_4$ was revealed by X-ray. The particle size was measured by TEM, being the values for the samples

with x = 0.2 and 0.4 of 45 and 80 nm, respectively. Ai & Jiang, 2010 prepared cobalt ferrite NPs by a one-step sol-gel auto-combustion method. It was found that the particle size and magnetic properties of the samples showed a strong dependence to the annealing temperature. The samples heat-treated at 700 °C seem as quasi-spheres with the crystallite size in the range of 25 - 30 nm.

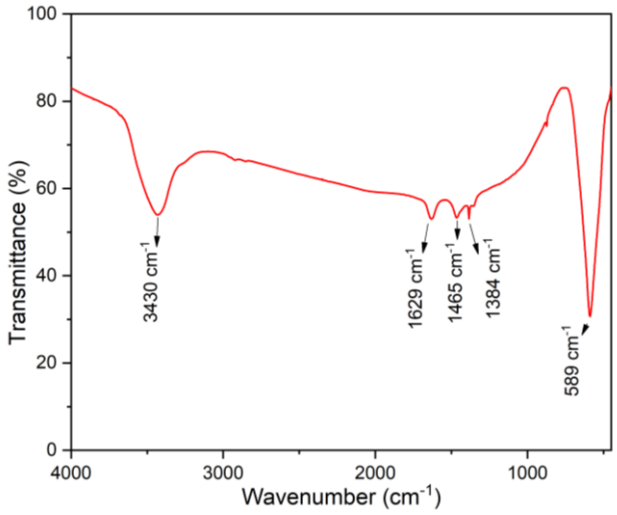

Figure 3. FTIR spectra of $CoFe_2O_4$@void@C.

The bands of the FTIR spectra (Figure 3) of $CoFe_2O_4$@void@C were compared and analyzed according to the literature of cobalt ferrite nanomaterials (Bagade *et al.*, 2017; Hamdi El Najjar *et al.*, 2014; Wang *et al.*, 2014). The strong band at 589 cm^{-1} confirms the metal oxide in the spinel structure due to the stretching vibrations of metal oxide in the octahedral group complex Co(II)-O^{2-} of the cobalt ferrite phase. The band observed at 3430 cm^{-1} is attributed to the O-H stretching vibrations and the absorption band present at 1629 cm^{-1} is due to the bending of the absorbed water molecules. Meanwhile, the band at 1465 cm^{-1} is due to the symmetric C-H stretching vibrations.

3.2. Performance of ferrite nanocatalyst in CWPO

The efficiency of the $CoFe_2O_4$ magnetic core and of $CoFe_2O_4$@void@C as catalyst in the CWPO of PCM are addressed through the monitoring of the concentrations of PCM, H_2O_2, and TOC over reaction time, as depicted in Figure 4. Figure 5 shows the conversions of paracetamol, TOC, the efficiency of H_2O_2 consumption at 6 h of reaction, and the percentage of iron leached at 24 h of reaction. To confirm the activity of the catalysts, a non-catalytic run at the same operational conditions was performed.

As observed, both catalyst show activity in the CWPO of PCM. The decomposition of H_2O_2, shown in Figure 4(a), achieved values of 10%, 68%, and 85% after 24 h of reaction in the non-catalytic run, and in the runs with the catalysts $CoFe_2O_4$ and $CoFe_2O_4$@void@C, respectively.

Regarding the conversion of PCM, Figure 4(b) and Figure 5 reveal that the best-tested material is $CoFe_2O_4$@void@C, showing 99.5% of conversion after 6 h of reaction. As can be observed in Figure 4(c) and 5, the catalysts allow to obtain the highest conversions of TOC, agreeing with the conversion results obtained for PCM and H_2O_2. The core $CoFe_2O_4$ and $CoFe_2O_4$@void@C achieved mineralization values of 46% and 58%, respectively, after 24 h of reaction.

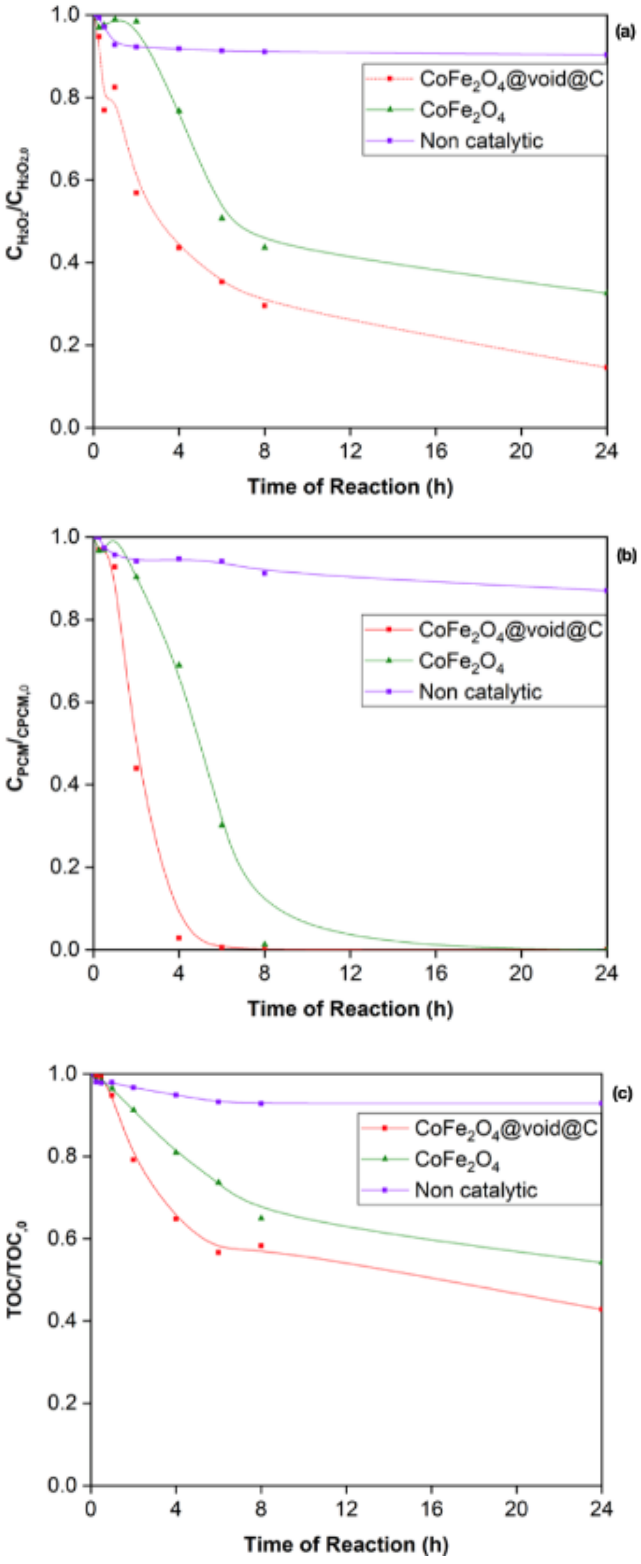

Figure 4. Normalized concentrations of (a) H_2O_2, (b) PCM and (c) TOC. (Operational conditions: $C_{PCM,0}$ = 0.6615 mmol·L^{-1}, $C_{H_2O_2,0}$ = 13.8881 mmol·L^{-1}, pH_0 = 3.5, 80°C). Lines connecting points are only intended to show the trend of concentration profiles.

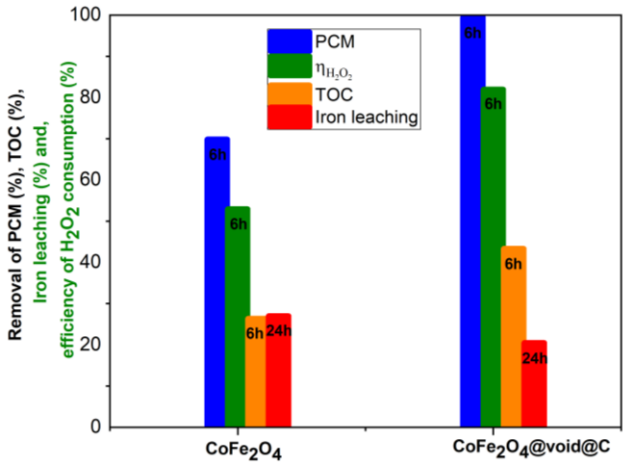

Figure 5. Removal of paracetamol, TOC and efficiency of H_2O_2 consumption at 6 h of reaction. % of Iron leached at 24 h of reaction. (Operational conditions: $C_{PCM,0}$ = 0.6615 mmol·L^{-1}, $C_{H_2O_2,0}$ = 13.8881 mmol·L^{-1}, pH_0 = 3.5, 80°C).

The absence of PCM adsorption over $CoFe_2O_4$ and $CoFe_2O_4$@void@C catalysts after 24 h of contact time was confirmed at the same operational conditions than those used in CWPO runs, evidencing that removals obtained though CWPO are due to the oxidation. The best performance of $CoFe_2O_4$@void@C as a catalyst when compared with the uncoated ferrite can be explained by the higher degree of crystallinity of the hybrid coated ferrite, as inferred from the peaks in the XRD pattern of the $CoFe_2O_4$@void@C sample, which increases significantly when compared to those of $CoFe_2O_4$. $CoFe_2O_4$@void@C also has a higher surface area, which also contributes to superior catalysis and its coated leading to runs of CWPO with a minimal amount of iron leaching.

Figure 5 shows that the $CoFe_2O_4$@void@C had lower amounts of iron leached. The determination of iron leached from the catalysts to the reaction solution was done after each CWPO run (24 h of reaction). As expected, the $CoFe_2O_4$@void@C material with the carbon-coated achieved a better result (iron leaching of 1.59 mg·L^{-1}) when compared to the uncoated ferrite which had an iron leaching of 2.54 mg·L^{-1}, value above the limit concentration of 2 mg·L^{-1} of iron in water established by European Union standards (Council Directive 98/83/EC).

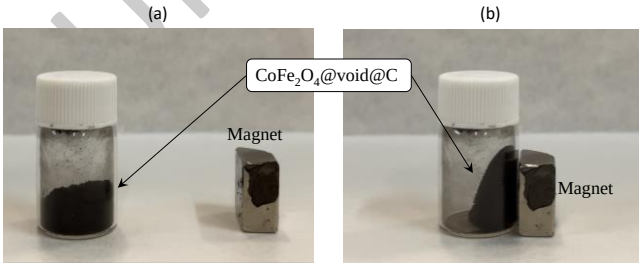

Figure 6. $CoFe_2O_4$@void@C catalysts (a) far and (b) close to the presence of a magnetic field.

The $CoFe_2O_4$@void@C catalyst produced by the sol-gel method described in this work shows high ferromagnetic behavior, even after the CWPO runs, as shown in Figure 6. During the coating process and the CWPO run, it is important to have a magnetic material to provide an abundant recovery of the samples. At the end of the oxidation reactions, it was possible to recover almost 100% of the catalyst using a magnetic field.

3.3. Kinetic modeling

3.3.1. PCM and H_2O_2 disappearance rates

To interpret the role of the oxidation reactions in the CWPO process, the kinetics were modeled from the results shown previously for the $CoFe_2O_4$@void@C as a catalyst. Considering the system as a batch reactor in a constant volume and perfect mixing, where an irreversible reaction occurs and that the composition of the aliquot taken at a given time was identical to the internal composition of the reactor at that time. It was also considered that adsorption was negligible in the whole process.

Different reaction rate equations have been proposed to fit the experimental data, namely first order, pseudo-first order, second order for each species and an autocatalytic-power-law kinetic model developed to predict the observed induction period and the dependence on the consumption of H_2O_2.

Due to lack of monitoring of the oxidation intermediates resulting from the oxidation of the model contaminant, only the rate of disappearance of PCM and H_2O_2 can be defined according to their concentrations, without taking into account the stoichiometry of the multiple reactions that can occur simultaneously, as shown in Eq. 1.

$$\boldsymbol{C_8H_9NO_2 + H_2O_2 \rightarrow non\ identified\ oxidized\ products + CO_2 + H_2O} \quad (1)$$

The kinetic study was done following the methodology proposed in other works that analyzed kinetic studies of oxidations reactions (Diaz de Tuesta *et al.*, 2017; Diaz de Tuesta *et al.*, 2019; Quintanilla *et al.*, 2019; Diaz de Tuesta *et al.*, 2019). The numerical integration of the rate equations presented in Table 2, with the initial conditions C_{PCM} = $C_{PCM,0}$, C_{H2O2} = $C_{H2O2,0}$ at t = 0 was solved by using the software Python 3.7 (Python Software Foundation, 2020, USA) to minimize the sum of squared errors (SSE) of the relative concentration of each compound i (rc_i = $C_i/C_{i,0}$) between the experimental (exp) and predicted (model) values, as given in Eq. 2.

$$\boldsymbol{SSE} = \sum_{n=1}^{N} (\boldsymbol{rc}_{\exp i,n} - \boldsymbol{rc}_{model\ i,n})^2 \quad (2)$$

The models were also evaluated by the determination factor (R^2) calculated by applying Eq. 3.

$$\boldsymbol{R}^2 = \frac{\sum_{n=1}^{N}(\mathrm{R}.C_{\mathrm{model\ i,n}} - \mathrm{R}.C^{-}_{\mathrm{model\ i}})^2}{\sum_{n=1}^{N}(\mathrm{R}.C_{\mathrm{model\ i,n}} - \mathrm{R}.C^{-}_{\mathrm{model\ i}})^2 + \sum_{n=1}^{N}(\mathrm{R}.C_{\mathrm{expi,n}} - \mathrm{R}.C_{\mathrm{model\ i,n}})^2} \quad (3)$$

where N in the total number of values (n) in a run and p is the number of predictors.

Table 2. Kinetic models considered to evaluate the disappearance rates of PCM and H_2O_2 in the CWPO run with $CoFe_2O_4$@void@C as catalyst (units in mmol and min).

No.	Kinetic model	Parameters	R^2	*SSE*
1	$\frac{dC_{H_2O_2}}{dt} = -k_{H_2O_2} C_{H_2O_2}$	$k_{H_2O_2}$= 0.0033 min^{-1}	0.95	0.118
2	$\frac{dC_{PCM}}{dt} = -k_{PCM} C_{PCM}$	k_{PCM} = 0.0064 min^{-1}	0.90	0.264
3	$\frac{dC_{H_2O_2}}{dt} = -k_{H_2O_2} C_{H_2O_2}^{\ 2}$	$k_{H_2O_2}$ = 0.00040 $L \cdot mmol^{-1} \cdot min^{-1}$	0.98	0.033
4	$\frac{dC_{PCM}}{dt} = -k_{PCM} C_{PCM}^{\ 2}$	k_{PCM} = 0.0148 $L \cdot mmol^{-1} \cdot min^{-1}$	0.67	0.583
6	$\frac{dC_{H_2O_2}}{dt} = -k_{H_2O_2} C_{H_2O_2}$	k_{H2O2} = 0.0033 min^{-1}	0.95	0.063
	$\frac{dC_{PCM}}{dt} = -k_{PCM} C_{PCM}$	k_{PCM} = 0.0624		
	$(C_0 - C_{PCM})$	$L \cdot mmol^{-1} \cdot min^{-1}$		
		C_0 = 0.6855 $mmol \cdot L^{-1}$		
7	$\frac{dC_{H_2O_2}}{dt} = -k_{H_2O_2} C_{H_2O_2}$	k_{H2O2} = 0.0033 min^{-1}	0.94	0.335
	$\frac{dC_{PCM}}{dt} = -k_{PCM} C_{PCM}$	k_{PCM} =0.0064 $L^2 \cdot (mmol^2)^{-1} \cdot min^{-1}$		
	$(C_0 - C_{PCM}) C_{H_2O_2}$	C_0 = 0.6833 $mmol \cdot L^{-1}$		
8	$\frac{dC_{H_2O_2}}{dt} = -k_{H_2O_2} C_{H_2O_2}^{\ 2}$	k_{H2O2} =4.1 10^{-4} $L \cdot mmol^{-1} \cdot min^{-1}$	0.98	0.252
	$\frac{dC_{PCM}}{dt} = -k_{PCM} C_{PCM}$	k_{PCM} =0.007 $L^2 \cdot (mmol^2)^{-1} \cdot min^{-1}$		
	$(C_0 - C_{PCM}) C_{H_2O_2}$	C_0 = 0.6832 $mmol \cdot L^{-1}$		

Figure 7 exhibits the concentrations of H_2O_2 and PCM during the time of reaction. It is observed that the kinetic models of the first and second order for paracetamol did not represent well the experimental data, especially in the case of the second-order model (model Nº4).

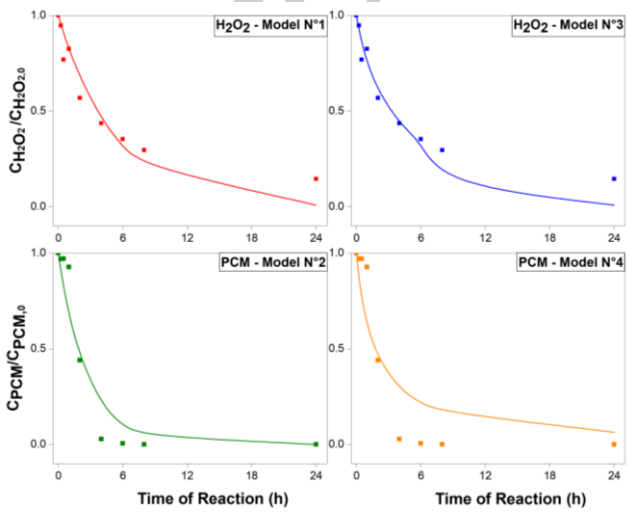

Figure 7. Experimental (symbols) and predicted (lines) concentrations of H_2O_2 (models 1 and 3) and PCM (models 2 and 4).

Regarding the disappearance of H_2O_2, the proposed second order power-law kinetic model (N°3) obtained a good representation of the values with a determination factor equal to 0.98.

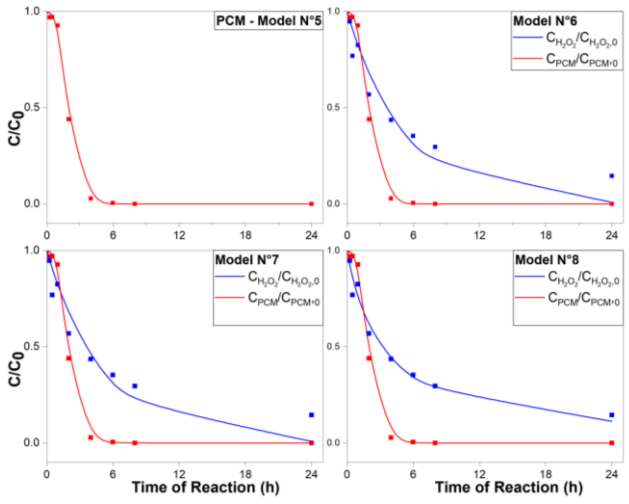

Figure 8. Experimental (symbols) and predicted (lines) concentrations of H_2O_2 and PCM.

The initial low-activity period of paracetamol can be well explained by the autocatalytic model, with a determination factor equal to 0.99, model N° 5 (Figure 8). Subsequently, the best models for the pollutants and oxidants were related together and the constant C_0 was determined. It is important to highlight that the value C_0 did not change significantly regardless of the proposed experimental models (0.6858, 0.6855, 0.6833, and 0.6832 mmol·L^{-1} for the models 5, 6, 7, and 8, respectively). From Table 2 and Figure 8 the model N° 8 achieved the best result in terms of R^2 and SSE. Thus, the CWPO of PCM with the $CoFe_2O_4$@void@C catalyst can be well-described by an empirical kinetic model composed of a second-order and an autocatalytic expression to describe the decomposition of H_2O_2 and PCM, respectively. In this sense, it is possible to predict the induction period, which takes place in the process.

Taking into account that there was no adsorption, there seems to be an oxidation process occurring at the surface of the carbon-shell promoting a higher catalytic activity, thus leading to an induction period. This behavior of carbon-based catalysts in oxidation reactions has been reported in various publications (Diaz de Tuesta *et al.*, 2017; Enterría & Figueiredo, 2016; Zhu *et al.*, 2019) suggesting that the same phenomenon can be occurring in this process, as a possible explanation.

The kinetic behavior expressed in the model's equations above is in alignment with previous research on oxidation reaction applying an iron-supported catalyst. Van *et al.*, 2020 tested a catalyst derived from iron slag (Fe-S) that was used for heterogeneous Fenton oxidation (H_2O_2/Fe-S) of paracetamol in a range of concentrations between 100 and 500 mg·L^{-1} in an aqueous solution. Kinetic experiments showed that the degradation of paracetamol occurs better when the concentration of PCM equals 100 mg·L^{-1} and was well fitted with a pseudo-first-order kinetic model. The calculated constant k was 0.0425 min^{-1}. Some of the reasons why the authors achieved such a different value for the kinetic constant is because they reported an adsorption process of paracetamol at the surface of Fe-S, while in this work the adsorption run did not show significant removal of pollutant.

Diaz de Tuesta *et al.*, 2019 performed work to understand the condensation by-products in CWPO processes in the absence of a catalyst but in presence of oxygen to the treatment of phenol. The authors proposed different equations to fit the experimental data. The models of pseudo-first-order, Langmuir-Hinshelwood-Hougen-Watson (LHHW), and autocatalytic rate were tested. However, the first two models did not consider the presence of an induction period in the concentration profiles of the three variables (phenol, H_2O_2, and TOC). On the other hand, the autocatalytic model provides a good fit because it takes into account the activity promoted by the condensation by-products formed during the reaction.

3.4. TOC abatement rate

After completing a review of different methods to describe TOC kinetics (Diaz de Tuesta *et al.*, 2019; Quintanilla *et al.*, 2019; Sun *et al.*, 2020), a model was proposed considering the total TOC as the sum of the different compounds produced during CWPO, as defined in Eq. 3.

$$TOC = TOC_A + TOC_B + TOC_C \quad (3)$$

where TOC_A corresponds to the TOC of PCM, TOC_B refers the oxidized intermediates resulting from the initial pollutant, which are still oxidized to refractory compounds represented by TOC_C. Specifically, TOC_C represents those compounds that do not oxidize and remain in the reaction medium. Hence, equations 4 to 7 represent the reaction pathway.

$$\frac{dC_{H_2O_2}}{dt} = -k_{H_2O_2} C_{H_2O_2}^{\ 2} \quad (4)$$

$$\frac{dC_{TOC,A}}{dt} = -k_1 C_{TOC,A}(C_0 - C_{TOC,A}) C_{H_2O_2} \quad (5)$$

$$\frac{dC_{TOC,B}}{dt} = k_2 C_{TOC,A}\left(C_0 - C_{TOC,A}\right) C_{H_2O_2} - k_3 C_{TOC,B} C_{H_2O_2} \quad (6)$$

$$\frac{dC_{TOC,C}}{dt} = k_4 C_{TOC,B} C_{H_2O_2} \quad (7)$$

To solve this model, the initial limit of integration was considered at t = 0, $TOC_{A,0} = TOC_0$, $TOC_A = TOC_{PCM}$, $TOC_{B,0}$ = 0 and $TOC_{C,0}$ = 0. The kinetics constants k_{H2O2}, k_1, and C_0 have been previously determined. To perform the TOC kinetics model, the values of the constants used were obtained in model N°8 (with $CoFe_2O_4$@void@C as a catalyst). Figure 9 shows the experimental and fitted data recorded by the proposed method. The calculated determination factor R^2 was 0.98 and the SSE equals 0.18.

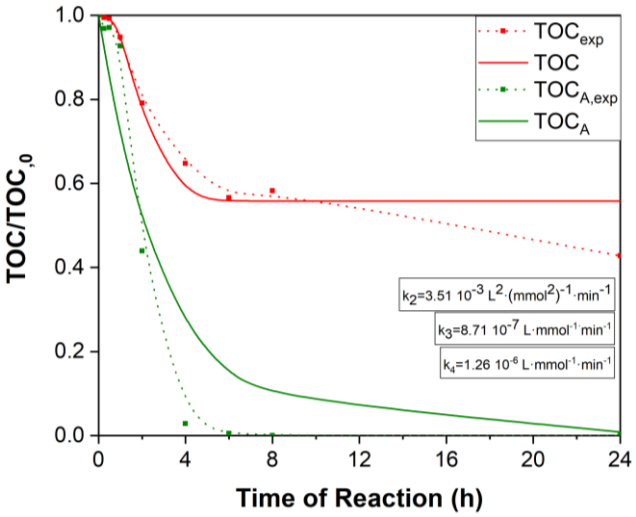

Figure 9. Experimental (dot lines) and predicted (lines) concentrations of TOC obtained in the CWPO of PCM (Operational conditions: $C_{PCM,0}$ = 0.6615 mmol·L^{-1}, $C_{H_2O_2,0}$ = 13.8881mmol·L^{-1}, pH_0 = 3.5, 80°C).

There are many approaches in how to describe a TOC kinetic model. However, to the best of our knowledge, there are no other works that describe the kinetic model

of concentration profiles of the TOC in the treatment of paracetamol by CWPO employing ferrites yolk-shell NPs as a catalyst.

Audino *et al.*, 2019 conducted a study on photo-induced oxidation for the treatment of 0.26 mmol·L^{-1} of paracetamol in a deionized water matrix, during a reaction span of 200 min. The authors fit the TOC concentration profile in a semi-empirical model. The kinetic was done calculating TOC in terms of conversion of the pollutant into CO_2 and H_2O. The *k* value calculated to achieve the maximum conversion was 0.007 min^{-1}.

Diaz de Tuesta *et al.*, 2017 developed a kinetic model with a commercial carbon black as a catalyst to describe the rate of H_2O_2 consumption and the targeted pollutant phenol degradation. The authors also took into account the total TOC as the sum of the different compounds produced during CWPO. Direct mineralization of phenol and the important selectivity of aromatic intermediates for mineralization have been reported instead of conversion into carboxylic acids as typically considered in wet oxidation studies of phenol.

4. Conclusions

Based on the premise of synthesizing yolk-shell magnetic NPs for application as catalysts in CWPO, this work considered the synthesis of $CoFe_2O_4$@void@C materials. XRD, TEM, and FTIR revealed that the core is composed of a $CoFe_2O_4$ cubic spinel structure with space group Fd-3m, with a crystallite size of 53 nm, calculated using the W-H method which is in agreement with the average size observed by TEM (53.51 ± 4.2 nm). The average size of the hybrid coated ferrite NPs increases to 58.7 ± 8.1 nm due to the coating introduced.

The treatment of waters containing paracetamol is promising when considering the CWPO process with $CoFe_2O_4$@void@C as a catalyst. The CWPO runs conducted revealed that over half of the paracetamol is converted in less than two hours of reaction. The CWPO of paracetamol with $CoFe_2O_4$@void@C led to a mineralization value of 58%. The $CoFe_2O_4$@void@C succeeds in avoiding iron leaching and proved to be a stable catalyst, the amount of iron at the end of the reaction being equal to 1.59 mg·L^{-1}.

The CWPO of PCM with the $CoFe_2O_4$@void@C catalyst can be well-described by an empirical kinetic model composed of a second-order and an autocatalytic expression that describe the decomposition of H_2O_2 and PCM, respectively. In this sense, it is possible to predict the induction period, which takes place in the process. The kinetic model of TOC can be well-described as the sum of the initial pollutant plus the oxidation intermediates from the PCM and the organic components that are refractory to the process.

CRediT authorship contribution statement

Nathália M. C. Guari: Investigation, Formal analysis, Writing - Original draft preparation. **Adriano Santos Silva**: Investigation, Methodology, Validation, Formal analysis. **Jose L. Diaz de Tuesta**: Methodology, Formal analysis, Visualization, Writing - Review & Editing, Supervision. **Walmir E. Pottker**: Methodology. **Patricia Y. Cordeiro**: Supervision. **Helder T. Gomes**: Supervision, Conceptualization, Writing - Reviewing and Editing, Funding acquisition.

Declaration of competing interest

The authors declare that they have no known competing financial interests or personal relationships that could have appeared to influence the work reported in this paper.

Acknowledgements

The authors are grateful to the Foundation for Science and Technology (FCT, Portugal) and FEDER (Fundo Eropeu de Desenvolvimento Regional) under Programme PT2020 for financial support to CIMO (UIDB/00690/2020). Adriano dos Santos Silva acknowledges the national funding by FCT and MIT Portugal Program for his individual research grant with reference number of SFRH/BD/151346/2021.

References

2015/495, C. I. D. (Eu), and 2015, of 20 M. (2015). COMMISSION IMPLEMENTING DECISION (EU) 2015/495 of 20 March 2015 establishing a watch list of substances for Union-wide monitoring in the field of water policy pursuant to Directive 2008/105/EC of the European Parliament and of the Council. *Official Journal of the European Union*, **L78/40**(C(2015) 1756), 20–30.

Ai L., and Jiang J. (2010). Influence of annealing temperature on the formation, microstructure and magnetic properties of spinel nanocrystalline cobalt ferrites. *Current Applied Physics*, **10**(1), 284–288. https://doi.org/10.1016/j.cap.2009.06.007.

Audino F., Santamaria J.M.T., Del Valle Mendoza L.J., Graells M., and Pérez-Moya M. (2019). Removal of paracetamol using effective advanced oxidation processes. *International Journal of Environmental Research and Public Health*, **16**(3). https://doi.org/10.3390/ijerph16030505.

Bagade A.A., Ganbavle V.V., Mohite S.V., Dongale T.D., Sinha B.B., and Rajpure K.Y. (2017). Assessment of structural, morphological, magnetic and gas sensing properties of $CoFe_2O_4$ thin films. In *Journal of Colloid and Interface Science,* **497**. https://doi.org/10.1016/j.jcis.2017.02.067.

Cai C., Kang S., Xie X., Liao C., Duan X., and Dionysiou D.D. (2020). Efficient degradation of bisphenol A in water by heterogeneous activation of peroxymonosulfate using highly active cobalt ferrite nanoparticles. *Journal of Hazardous Materials*, **399**, 122979. https://doi.org/https://doi.org/10.1016/j.jhazmat.2020.122979.

Desai S.S., Shirsath S.E., Mujasam Batoo K., Adil S.F., Khan M., and Patange S.M. (2020). Influence of Zn-Zr substitution on the crystal chemistry and magnetic properties of $CoFe_2O_4$ nanoparticles synthesized by sol-gel method. *Physica B: Condensed Matter*, **596**(March), 412400. https://doi.org/10.1016/j.physb.2020.412400.

Diaz de Tuesta J.L., de Almeida F.V.M., Oliveira J.R.P., Praça P., Guerreiro M.C., and Gomes H.T. (2021). Kinetic insights on wet peroxide oxidation of caffeine using EDTA-functionalized low-cost catalysts prepared from compost generated in municipal solid waste treatment facilities. *Environmental Technology & Innovation*, **24**, 101984. https://doi.org/10.1016/j.eti.2021.101984.

Diaz de Tuesta J.L., Quintanilla A., Casas J.A., Morales-Torres S., Faria J.L., Silva A.M.T., and Gomes H.T. (2020). The pH effect on the kinetics of 4-nitrophenol removal by CWPO with doped carbon black catalysts. *Catalysis Today*, **356**, 216–225. https://doi.org/10.1016/j.cattod.2019.08.033.

Diaz de Tuesta J.L., Quintanilla, A., Casas, J.A., and Rodriguez, J.J. (2017). Kinetic modeling of wet peroxide oxidation with a carbon black catalyst. *Applied Catalysis B: Environmental*, **209**, 701–710. https://doi.org/10.1016/j.apcatb.2017.03.031.

Diaz de Tuesta J.L., Quintanilla A., Moreno D., Ferro V.R., and Casas J.A. (2020). Simulation and optimization of the CWPO process by combination of aspen plus and 6-factor doehlert matrix: Towards autothermal operation. *Catalysts*, **10**(5). https://doi.org/10.3390/catal10050548.

Dippong T., Deac I.G., Lazar M.D., Petean I., Levei E.A., Borodi G., and Cadar O. (2021). Effect of heat-treatment temperature and zinc addition on magnetostructural and surface properties of manganese nanoferrite prepared by an ecofriendly sol–gel synthesis. *Journal of Materials Research and Technology*, **15**, 6528–6540. https://doi.org/10.1016/j.jmrt.2021.11.073.

Duan Q., Lee J., Chen H., and Zheng Y. (2017). Preparation and catalytic performance of copper-containing magnetic catalysts for degradation of azo dye (direct violet). *Water Science and Technology*, **76**(11), 3069–3078. https://doi.org/10.2166/wst.2017.475.

Enterría M., and Figueiredo J.L. (2016). Nanostructured mesoporous carbons: Tuning texture and surface chemistry. *Carbon*, **108**, 79–102. https://doi.org/10.1016/j.carbon.2016.06.108.

Gadipelly C., Pérez-González A., Yadav G.D., Ortiz I., Ibáñez R., Rathod V.K., and Marathe K.V. (2014). Pharmaceutical industry wastewater: Review of the technologies for water treatment and reuse. *Industrial and Engineering Chemistry Research*, **53**(29), 11571–11592. https://doi.org/10.1021/ie501210j.

Giannakopoulou T., Kompotiatis L., Kontogeorgakos A., and Kordas G. (2002). Microwave behavior of ferrites prepared via sol-gel method. *Journal of Magnetism and Magnetic Materials*, **246**(3), 360–365. https://doi.org/10.1016/S0304-8853(02)00106-3.

Hall W.H. (1949). X-ray line broadening in metals [3]. *Proceedings of the Physical Society.Section A*, **62**(11), 741–743. https://doi.org/10.1088/0370-1298/62/11/110.

Hamdi El Najjar N., Touffet A., Deborde M., Journel R., and Karpel Vel Leitner N. (2014). Kinetics of paracetamol oxidation by ozone and hydroxyl radicals, formation of transformation products and toxicity. *Separation and Purification Technology*, **136**, 137–143. https://doi.org/10.1016/j.seppur.2014.09.004.

Heidari M.R., Varma R.S., Ahmadian M., Pourkhosravani M., Asadzadeh S.N., Karimi P., and Khatami M. (2019). Photo-Fenton like catalyst system: Activated Carbon/$CoFe_2O_4$ nano-composite for reactive dye removal from textile wastewater. *Applied Sciences*, **9**(5). https://doi.org/10.3390/app9050963.

Huaccallo-Aguilar Y., Álvarez-Torrellas S., Martínez-Nieves J., Delgado-Adámez J., Gil M.V., Ovejero G., and García J. (2021). Magnetite-based catalyst in the catalytic wet peroxide oxidation for different aqueous matrices spiked with naproxen–diclofenac mixture. *Catalysts*, **11**(4). https://doi.org/10.3390/catal11040514.

Huaccallo-Aguilar Y., Diaz de Tuesta J.L., Álvarez-Torrellas S., Gomes H.T., Larriba M., Ovejero G., and García J. (2021). New insights on the removal of diclofenac and ibuprofen by CWPO using a magnetite-based catalyst in an up-flow fixed-bed reactor. *Journal of Environmental Management*, **281**. https://doi.org/10.1016/j.jenvman.2020.111913

Kiani M., Tian X.Q., Kiani A.B., ur Rehman S., Khan S.A., Khan K., Tareen A.K., Khan Q.U., and Mahmood I. (2021). A first principle study: Effect of tin substitution on magnetic properties of bismuth ferrite nanoparticles prepared by sol-gel synthesis method. *Inorganic Chemistry Communications*, **127**, 108483. https://doi.org/10.1016/j.inoche.2021.108483.

Kim K.N., Jung H.R., and Lee W.J. (2016). Hollow cobalt ferrite-polyaniline nanofibers as magnetically separable visible-light photocatalyst for photodegradation of methyl orange. *Journal of Photochemistry and Photobiology A: Chemistry*, **321**, 257–265. https://doi.org/10.1016/j.jphotochem.2016.02.007.

Masudi A., Harimisa G.E., Ghafar N.A., and Jusoh N.W.C. (2020). Magnetite-based catalysts for wastewater treatment. *Environmental Science and Pollution Research*, **27**(5), 4664–4682. https://doi.org/10.1007/s11356-019-07415-w.

Munoz M., Mora F.J., de Pedro Z.M., Alvarez-Torrellas S., Casas J.A., and Rodriguez J.J. (2017). Application of CWPO to the treatment of pharmaceutical emerging pollutants in different water matrices with a ferromagnetic catalyst. *Journal of Hazardous Materials*, **331**, 45–54. https://doi.org/10.1016/j.jhazmat.2017.02.017.

Munoz M., Nieto-Sandoval J., Serrano E., de Pedro Z.M., and Casas J.A. (2020). CWPO intensification by induction heating using magnetite as catalyst. *Journal of Environmental Chemical Engineering*, **8**(5), 104085. https://doi.org/10.1016/j.jece.2020.104085.

Nath D., Singh F., and Das R. (2020). X-ray diffraction analysis by Williamson-Hall, Halder-Wagner and size-strain plot methods of CdSe nanoparticles- a comparative study. *Materials Chemistry and Physics*, **239**, 122021. https://doi.org/10.1016/j.matchemphys.2019.122021.

Oliveira J., Rodrigues R., Barros L., Ferreira I., Marchesi L., Koneracka M., Jurikova A., Zavisova V., and Gomes H.T. (2018). Carbon-Based Magnetic Nanocarrier for Controlled Drug Release: A Green Synthesis Approach. *C*, **5**(1), 1. https://doi.org/10.3390/c5010001.

Quintanilla A., Diaz de Tuesta J.L., Figueruelo C., and Munoz M. (2019). Condensation By-Products in Wet Peroxide Oxidation: Fouling or Catalytic Promotion? Part I. Evidences of an Autocatalytic Process. *Catalysts 2019*, **9**, 516. https://doi.org/10.3390/catal9060516.

Pullar R.C. (2012). Hexagonal ferrites: A review of the synthesis, properties and applications of hexaferrite ceramics. *Progress in Materials Science*, **57**(7), 1191–1334. https://doi.org/10.1016/j.pmatsci.2012.04.001.

Ribeiro R.S., Gallo J., Bañobre-López M., Silva A.M.T., Faria J.L., and Gomes H.T. (2019). Enhanced performance of cobalt ferrite encapsulated in graphitic shell by means of AC magnetically activated catalytic wet peroxide oxidation of 4-nitrophenol. *Chemical Engineering Journal*, **376**, 120012. https://doi.org/10.1016/j.cej.2018.09.173.

Ribeiro R.S., Rodrigues R.O., Silva A.M.T., Tavares P.B., Carvalho A.M.C., Figueiredo J.L., Faria J.L., and Gomes H.T. (2017). Hybrid magnetic graphitic nanocomposites towards catalytic wet peroxide oxidation of the liquid effluent from a mechanical biological treatment plant for municipal solid waste. *Applied Catalysis B: Environmental*, **219**, 645–657. https://doi.org/10.1016/j.apcatb.2017.08.013.

Ribeiro R.S., Silva A.M.T., Figueiredo J.L., Faria J.L., and Gomes H.T. (2016). Catalytic wet peroxide oxidation: a route towards the application of hybrid magnetic carbon nanocomposites for the degradation of organic pollutants. A review. *Applied Catalysis B: Environmental*, **187**, 428–460. https://doi.org/10.1016/j.apcatb.2016.01.033.

Rodrigues R., Baldi G., Doumett S., Gallo J., Bañobre-López M., Dražić G., Calhelha R., Ferreira I., Lima R., Silva A., and Gomes H.T. (2018). A tailor-made protocol to synthesize yolk-shell graphene-based magnetic nanoparticles for nano-medicine *C*, **4**(4), 55. https://doi.org/10.3390/c4040055.

Rodrigues R.O., Baldi G., Doumett S., Garcia-hevia L., Gallo J., Bañobre-lópez M., Dra G., Calhelha R.C., Ferreira I.C.F.R., Lima R., Gomes H.T., and Silva A.M.T. (2018). Multifunctional graphene-based magnetic nanocarriers for combined hyperthermia and dual stimuli-responsive drug delivery. *Materials Science & Engineering C*, **93**, 206–217. https://doi.org/10.1016/j.msec.2018.07.060.

Senapati K.K., Borgohain C., and Phukan P. (2012). $CoFe_2O_4$-ZnS nanocomposite: A magnetically recyclable photocatalyst. *Catalysis Science and Technology*, **2**(11), 2361–2366. https://doi.org/10.1039/c2cy20400b.

Silva A.S., Kalmakhanova M.S., Massalimova B.K., Diaz de Tuesta J.L., and Gomes H.T. (2019). Wet peroxide oxidation of paracetamol using acid activated and Fe/Co-pillared clay catalysts prepared from natural clays. *Catalysts*, **9**(9). https://doi.org/10.3390/catal9090705.

Sun M., Hong X.H., Tao X.F., Zhai L.F., and Wang S. (2020). A generalized kinetic model for electro-assisted catalytic wet air oxidation of triclosan on Ni@NiO/graphite electrode. *Chemical Engineering Science*, **222**, 115696. https://doi.org/10.1016/j.ces.2020.115696.

Van H.T., Nguyen L.H., Hoang T. K., Nguyen T. T., Tran T. N. H., Nguyen T. B. H., Vu X. H., Pham M. T., Tran T. P., Pham T. T., Nguyen H. D., Chao H. P., Lin C. C., and Nguyen X. C. (2020). Heterogeneous Fenton oxidation of paracetamol in aqueous solution using iron slag as a catalyst: Degradation mechanisms and kinetics: Iron slag-based heterogeneous Fenton degradation of paracetamol. *Environmental Technology and Innovation*, **18**, 100670. https://doi.org/10.1016/j.eti.2020.100670.

Wang B., Gao C., Wang W., Kong F., and Zheng C. (2014). TGA-FTIR investigation of chemical looping combustion by coal with $CoFe_2O_4$ combined oxygen carrier. *Journal of Analytical and Applied Pyrolysis*, **105**, 369–378. https://doi.org/10.1016/j.jaap.2013.12.002.

Zhang Q., Cheng S., Xia H., Zhang L., Zhou J., Li C., Shu J., and Jiang X. (2019). Paracetamol Degradation Performance and Mechanisms Using Microwave-Assisted Heat-Activated Persulfate in Solutions. *Water, Air, and Soil Pollution*, **230**(12). https://doi.org/10.1007/s11270-019-4286-7.

Zhang Y., Yang Z., Yin D., Liu Y., Fei C., Xiong R., Shi J., and Yan G. (2010). Composition and magnetic properties of cobalt ferrite nano-particles prepared by the co-precipitation method. *Journal of Magnetism and Magnetic Materials*, **322**(21), 3470–3475. https://doi.org/10.1016/j.jmmm.2010.06.047.

Zhu Y., Zhu R., Xi Y., Zhu J., Zhu G., and He H. (2019). Strategies for enhancing the heterogeneous fenton catalytic reactivity: A review. *Applied Catalysis B: Environmental*, **255**(May), 117739. https://doi.org/10.1016/j.apcatb.2019.05.041.